

MYC Induces Immunotherapy and IFN γ Resistance Through Downregulation of JAK2

Ettai Markovits^{1,2}, Ortal Harush^{1,2}, Erez N. Baruch^{1,2}, Eldad D. Shulman³, Assaf Debby^{4,5}, Orit Itzhaki¹, Liat Anafi⁴, Artem Danilevsky⁶, Noam Shomron⁶, Guy Ben-Betzalel¹, Nethanel Asher¹, Ronnie Shapira-Frommer¹, Jacob Schachter^{1,6}, Iris Barshack^{4,6}, Tamar Geiger³, Ran Elkon³, Michal J. Besser^{1,2,7,8}, and Gal Markel^{2,7}



ABSTRACT

Immunotherapy has revolutionized the treatment of advanced melanoma. Because the pathways mediating resistance to immunotherapy are largely unknown, we conducted transcriptome profiling of preimmunotherapy tumor biopsies from patients with melanoma that received PD-1 blockade or adoptive cell therapy with tumor-infiltrating lymphocytes. We identified two melanoma-intrinsic, mutually exclusive gene programs, which were controlled by IFN γ and MYC, and the association with immunotherapy outcome. MYC-overexpressing melanoma cells exhibited lower IFN γ responsiveness, which was linked with

JAK2 downregulation. Luciferase activity assays, under the control of JAK2 promoter, demonstrated reduced activity in MYC-overexpressing cells, which was partly reversible upon mutagenesis of a MYC E-box binding site in the JAK2 promoter. Moreover, silencing of MYC or its cofactor MAX with siRNA increased JAK2 expression and IFN γ responsiveness of melanomas, while concomitantly enhancing the effector functions of T cells coincubated with MYC-overexpressing cells. Thus, we propose that MYC plays a pivotal role in immunotherapy resistance through downregulation of JAK2.

Introduction

In recent years, the field of immunotherapy has joined the ranks of surgery, radiation, chemotherapy, and targeted therapy as a pillar of cancer therapy (1). Most cancer immunotherapies are based on the unique characteristics of T cells. These cells can distinguish between tumors and normal tissue by recognizing tumor-specific antigens and can generate immune memory. Primary T-cell responses are generally followed by the production of long-lived memory T cells that exhibit accelerated kinetics of secondary responses upon antigen reexposure (2). Immunotherapy has proven efficacy in multiple types of cancer, including lung, bladder, renal cancer, and melanoma (3). Melanoma is considered as an immunogenic tumor, expressing a variety of tumor neoantigens arising from ultraviolet-induced somatic mutations (4). Therefore, it is not surprising that immunotherapy has revolutionized the treatment in advanced melanoma—the 5-year survival rate of patients with metastatic melanoma has improved from

less than 5% to more than 40% with the introduction of new immunotherapies, such as monoclonal anti-CTLA-4 and anti-PD-1 (5).

Adoptive cell transfer (ACT) with tumor-infiltrating lymphocytes (TIL) is another type of immunotherapy, which demonstrates tumor regressions in 50% of patients with advanced melanoma (6, 7), with responding patients exhibiting a median survival greater than 50 months in contrast to median survival of 6.1 months in nonresponders (8). However, although immunotherapy vastly improves the prognosis of patients with advanced melanoma, the majority of patients treated with immunotherapy will exhibit primary or secondary resistance to immunotherapy, entailing disease progression. Therefore, in recent years, there has been an ongoing effort to unveil factors related to response and resistance to immunotherapy. Although there is a growing consensus that high mutational burden (9), tumor immune infiltration (10), and IFN γ signaling (11, 12) all associate with higher response rates to immunotherapy, the mechanisms that induce resistance to immunotherapy are largely unknown. Moreover, although a few recent articles identify immunotherapy resistance mechanisms, such as alterations in the IFN γ and antigen presentation pathways (13) and activation of oncogenic pathways that mediate immune exclusion (14–16), there are no available treatments targeting these resistance mechanisms that exhibit clinical efficacy. Thus, it is of utmost importance to improve our understanding of the pathways underlying response and resistance to immunotherapy, to enable development of new treatment combinations and to better select patients who will benefit from immunotherapy.

To further investigate the mechanisms that govern the response and resistance to immunotherapy, we profiled the proteomes and transcriptomes of pretreatment tumor biopsies from patients with advanced melanoma treated with immunotherapy. In a recent article by Harel and colleagues, we observed an increase in oxidative metabolism in the proteomes of responding patients to immunotherapy, which associated with increased melanoma immunogenicity through upregulation of antigen presentation machinery (17). Here, we report the identification of two mutually exclusive gene programs in transcriptomes of immunotherapy-treated patients that are regulated by

¹Ella Lemelbaum Institute for Immuno-oncology, Sheba Medical Center, Tel Hashomer, Israel. ²Department of Clinical Microbiology and Immunology, The Sackler School of Medicine, Tel Aviv University, Tel-Aviv, Israel. ³Department of Human Molecular Genetics and Biochemistry, The Sackler School of Medicine, Tel Aviv University, Tel-Aviv, Israel. ⁴Institute of Pathology, Sheba Medical Center, Tel Hashomer, Israel. ⁵Department of Dermatology, Sheba Medical Center, Tel Hashomer, Israel. ⁶Sackler School of Medicine, Tel Aviv University, Tel Aviv, Israel. ⁷Davidoff Cancer Center, Rabin Medical Center-Beilinson Hospital, Petah Tikva, Israel. ⁸Felsenstein Medical Research Center, Rabin Medical Center-Beilinson Hospital, Petah Tikva, Israel.

E. Markovits and O. Harush contributed equally to this article.

Corresponding Authors: Gal Markel, Davidoff Center, Rabin Medical Center, Petah Tikva 11111, Israel. E-mail: galma4@clalit.org.il; and Ettai Markovits, ettaim@mail.tau.ac.il

Cancer Immunol Res 2023;11:909–24

doi: 10.1158/2326-6066.CIR-22-0184

©2023 American Association for Cancer Research

IFN γ and MYC and the relationship to clinical outcome of patients with advanced melanoma treated with immunotherapy. Moreover, we demonstrate that MYC can induce IFN γ and immunotherapy resistance through transcriptional repression of the IFN γ signaling protein JAK2.

Materials and Methods

Tumor tissue collection from patients

For the TIL adoptive cell transfer (ACT) cohort, we collected formalin-fixed, paraffin-embedded (FFPE) pretreatment tumor biopsies from 37 patients with advanced melanoma treated with TIL ACT. A total of 36 patients were treated with the “Young”-TIL protocol, whereas 1 patient was treated with the “Selected”-TIL protocol (18). None of the included TIL ACT patients were previously treated with PD-1 blockade. Response to therapy indicates best overall response, as defined by RECIST v1.0. For the PD-1 blockade cohort, we collected FFPE pretreatment tumor biopsies from 36 patients with advanced melanoma treated with either nivolumab or pembrolizumab. Response to therapy indicates best overall response according to multidisciplinary radiologic evaluations. Written informed consent was obtained from all patients, and all studies were conducted in accordance with the Declaration of Helsinki, approved by the Institutional Review Board and by the Israeli Ministry of Health (approval no. 3518/2004).

RNA sequencing and dataset analysis

RNA from preimmunotherapy FFPE tumor biopsies of patients with advanced melanoma was extracted with RNeasy FFPE Kit (Qiagen, catalog no. 73504). RNA sequencing (RNA-seq) libraries were prepared with Illumina’s Ribo Zero Gold and TruSeq stranded library prep kits and sequenced on the Illumina HiSeq2500 platform using paired-end sequencing with read length of 2×125 –150 bps. Reads were aligned to the human genome reference build hg38 using STAR aligner (19) and were quantified with FeatureCounts (20). After filtration of lowly expressed genes (counts below 10 in more than 90% of samples), raw counts were normalized and analyzed in the R environment according to the LIMMA pipeline (21).

Published RNA-seq datasets of patients with melanoma treated with PD-1 blockade (GSE91061; ref. 22) and TIL ACT (GSE100797; ref. 23) were downloaded from the Gene Expression Omnibus (GEO) database and github (<https://github.com/vanallenlab/schadendorf-pd1>; ref. 12). Raw sequencing data from two PD-1 blockade-treated cohorts (10, 24) were downloaded from the Sequence Read Archive (PRJNA312948) and European Nucleotide Archive (PRJEB23709) and processed as mentioned above. A melanoma single-cell (sc) RNA-seq dataset (16, 25) was downloaded from the GEO database (GSE115978). RSEM raw counts of The Cancer Genome Atlas skin cutaneous melanoma (TCGA SKCM) dataset were downloaded from FireBrowse (<http://firebrowse.org>) and processed as mentioned above.

Dataset analysis to compare proteomic and transcriptomic profiles

For patients with available transcriptomic and proteomic (17) data from the same tumor biopsy ($n = 73$), raw proteomic data were downloaded (<https://ars.els-cdn.com/content/image/1-s2.0-S0092867419309006-mm1.xlsx>) and lowly detected proteins (proteins detected in less than 10% of samples) were filtered out as indicated above. For discovery of a potential bias in the proteomic data toward detection of highly expressed genes, we first assessed gene expression

by averaging the transcripts per million (TPM) of each transcript. Next, we compared the detection probability, calculated as $P_{detection} = \frac{n \text{ genes detected in proteomics and RNAseq}}{n \text{ genes detected in RNAseq}}$, of high and low abundance genes (above and below the median of the average TPM). To assess detection of proteins and mRNA expressed by melanoma, stromal, and immune cells, we calculated the detection probability of previously published melanoma, stroma, and immune cell markers (16) in our proteomic and transcriptomic data. Finally, we assessed the dependency between mRNA expression and protein levels by correlating the \log_2 TPM values and the proteomic \log_2 -transformed ratio between the tumor samples and an internal control composed of five SILAC (stable isotope labeling with amino acids)-labeled melanoma cell lines obtained from the same tumor biopsies (17).

Transcriptome profiling of responders and nonresponders to immunotherapy

To identify the sources of intersample variability in our transcriptomic data, we performed principal component analysis on the 3,000 most variable genes after variance-stabilizing transformation of filtered raw counts and removal of batch effect between the TIL ACT and PD-1 cohorts by the *removebatcheffect* function in the LIMMA package. The first two principal components were correlated with the normalized expression of all quantified genes and with the ImmuneScore, a method based on gene expression signatures to infer the fraction of immune cells in tumor samples (26). To assess the similarity between response and resistance mechanisms to TIL ACT and PD-1 blockade, we correlated the \log_2 fold change of the top 500 differentially expressed genes (DEG) between responders (complete or partial response) and nonresponders (stable or progressive disease) to these treatments; and gene set enrichment analysis (GSEA; ref. 27) normalized enrichment scores of differentially expressed Hallmark gene sets (FDR < 0.05; ref. 28). For identification of global response and resistance mechanisms to immunotherapy, we compared the transcriptomes of responders and nonresponders with TIL ACT and PD-1 blockade using the R package LIMMA pipeline, with voom normalization and blocking for cohort in the design matrix (21). Normalized and batch-corrected expression of DEGs was visualized using the R package pheatmap. DEGs and sample cluster identification was performed with Ward’s hierarchical agglomerative clustering.

Assessment of tumor cell composition from transcriptomic data in responders and nonresponders to immunotherapy was performed with xCell (29), a gene signature-based method for inference of the tumor immune and stromal cell composition. To estimate which cells within the tumor expressed the three identified gene clusters, we averaged and standardized the \log_2 -transformed TPM values of each cluster gene by cell type in a melanoma scRNA dataset (GSE115978; refs. 16, 25). To inspect the relationship between the three gene clusters—Melanoma response, Melanoma resistance, and Lymphocyte markers; identified by hierarchical clustering of the DEGs (see Results), we correlated the gene cluster scores, computed by Gene Set Variation Analysis (GSVA; ref. 30), for each sample in our own TIL ACT and PD-1 cohort ($n = 73$) and in a combined cohort ($n = 356$) of metastatic samples from TCGA SKCM dataset and previously published melanoma RNA-seq datasets (10, 12, 22–24). To investigate the correlation between the three clusters by cell type, we computed the overall expression score of each cluster in a melanoma scRNA dataset (GSE115978; refs. 16, 25).

To assess the effect of the melanoma-intrinsic immunotherapy resistance and response programs on treatment outcome, we compiled the “Melanoma Immunotherapy Resistance Score” (MIRScore) by

subtracting the Melanoma response cluster score from the Melanoma resistance cluster score, both calculated by GSVA on the Melanoma response and Melanoma resistance cluster genes. Next, we compared 5-year survival between patients with high (above median) and low (below median) MIRScore, Lymphocyte markers cluster score, calculated by GSVA on the Lymphocyte markers cluster genes, and ImmuneScore in our own TIL ACT and PD-1 blockade cohorts ($n = 73$) for both mRNA and protein levels [after filtration for proteins which highly correlated with mRNA expression ($r_p > 0.4$)], as well as in a combined immunotherapy cohort ($n = 288$) of previously published PD-1 blockade (10, 12, 22, 24) and TIL ACT (23) cohorts.

Characterization of the Melanoma response and resistance gene clusters in a combined melanoma RNA-seq dataset

To better characterize the Melanoma response and resistance cell states, we compiled a combined melanoma dataset ($n = 403$), comprised of seven melanoma RNA-seq datasets with available raw counts—our own TIL ACT ($n = 37$) and PD-1 blockade ($n = 36$) datasets, metastatic samples from TCGA SKCM dataset ($n = 68$), and four previously published PD-1 blockade dataset—Hugo and colleagues ($n = 27$), Riaz and colleagues ($n = 47$), Gide and colleagues ($n = 73$), and Liu and colleagues ($n = 115$; refs. 10, 12, 22, 24). Next, we compared between the transcriptomes of MIRScore^{high} (upper third, $n = 134$) and MIRScore^{low} (lower third, $n = 135$) tumors in the combined melanoma dataset. Visualization and clustering of the top 1,000 DEGs was performed, as described above, which resulted again in three distinct clusters of DEGs. We then assessed the similarity between the newly and previously identified three gene clusters by correlating their cluster scores in the combined datasets. For identification of upstream regulators associated with the MIRScore^{high} and MIRScore^{low} phenotypes, we performed Ingenuity upstream regulator analysis (QIAGEN) on the top 1,000 differentially expressed genes between the MIRScore^{high} and MIRScore^{low} tumors (FDR < 0.01 and absolute log₂ fold change > 1.5).

MYC activity in pretreatment biopsies from responders and nonresponders to PD-1 blockade

To validate increased MYC activity in nonresponders to immunotherapy, we performed MYC staining (antibodies used listed in Supplementary Table S1A) on tissue microarrays composed of pretreatment biopsies of patients with advanced melanoma treated with PD-1 blockade ($n = 35$). Each tissue sample from each patient was initially stained with hematoxylin and eosin (H&E), and representative areas of tumors were marked by an expert pathologist morphologically. Accordingly, three 2-mm-diameter tissue cylinders were punched out from each tumor block and deposited into a recipient block using Manual Tissue Arrayer MTA-1 (Beecher Instruments Inc.). Tumor sample triplicates were used as a means of overcoming tumor heterogeneity. After array construction, a 4 μm section was H&E stained to confirm the histologic quality. A consecutive 4 μm section was used for IHC MYC staining. Quantification of MYC staining intensity (from 0 to 5) in the nucleus or cytoplasm of tumor cells was performed by a blinded expert pathologist with a bright-field microscope (Olympus). High MYC staining was defined as staining intensity ≥ 2 in at least one tissue core. Uninterpretable cores due to loss of the tissue or excessive background staining were excluded from the analyses. This study was approved by the Institutional Review Board of Sheba Medical Center (Protocol SMC-2406). Moreover, we assessed samples using GSVA (30) for the expression of Hallmark MYC target gene sets, downloaded from the Molecular Signatures

Database (<https://www.gsea-msigdb.org/gsea/msigdb/>), in responders ($n = 22$) and nonresponders ($n = 14$) to PD-1 blockade.

Profiling of the Melanoma response and resistance gene clusters in TCGA database

To further investigate the relationship between the Melanoma response and resistance gene clusters in other malignancies, we downloaded from the cBio cancer genomics portal (31) available RNA-seq and reverse phase protein array (RPPA) datasets for all TCGA tumor types. Next, for each tumor type, we computed the correlation between the cluster scores, computed by averaging the normalized and standardized expression of the Melanoma response and resistance gene clusters identified in the combined melanoma datasets analysis. For identification of proteins associated with the MIRScore^{high} phenotype, we computed the MIRScore for each sample in TCGA SKCM cohort by GSVA and compared RPPA protein expression in MIRScore^{high} (upper third, $n = 117$) and MIRScore^{low} tumors (lower third, $n = 117$).

Pathway enrichment analysis for genes inversely correlated with JAK2 expression

To verify that the MYC transcriptional program was inversely correlated to JAK2 in the combined melanoma dataset ($n = 403$), we performed Hallmark pathway enrichment analysis for genes inversely correlated to JAK2 ($r_p < -0.6$, $n = 402$) using a hypergeometric test. Hallmark gene sets were downloaded from the Molecular Signatures Database as indicated above.

Cells and media

Patient-derived melanoma cell lines Mel 53, Mel 90, Mel 111, Mel 131 (all obtained from surgically excised melanoma specimens of TIL ACT-treated patients in our institute between 2008 and 2012) and Mel 526 (obtained from Dr. Steve A. Rosenberg, NCI, Bethesda, MD) were maintained in RPMI1640 medium (Biological Industries, catalog no. 01-100-1A) supplemented with 10% FBS (Biological Industries, catalog no. 04-127-1A). Primary bulk TIL cultures TIL53, TIL90, and TIL 111 were obtained from surgically excised melanoma specimens in our institution following a rapid expansion protocol, and cells were cryopreserved as described previously (32). A total of 72 hours prior to functional experiments, TIL cultures were thawed and maintained in RPMI1640 medium supplemented with 10% FBS, 0.05 mmol/L β -mercaptoethanol (Gibco, catalog no. 21985023), and 3,000 units/mL of IL2 (rhIL2, Novartis, catalog no. 3000014936). 293T cells (ATCC) were maintained in DMEM (Biological Industries, catalog no. 01-055-1A) with 10% FBS. All cell lines were cultured for up to 2 months after thawing and were tested routinely for *Mycoplasma* (Hy-Mycoplasma Kit, Hylabs, catalog no. KI50341).

Generation of stable overexpression cell systems

The MYC overexpression vector was cloned into the pQCXIP.puro vector using the Gibson Assembly Master Mix (NEB, catalog no. E2611). Transfection of 293T cells was performed using TurboFect Transfection Reagent (catalog no. R0531, Thermo Fisher Scientific) according to the manufacturer protocol. Melanoma cell infection with virion-containing medium was performed as described previously (33). After infection, selection was performed by addition of 1 μg/mL puromycin (Merck Millipore, catalog no. 540411) into culture medium. All transfected cell lines were tested routinely for MYC overexpression by qRT-PCR and Western blot analysis (see Supplementary Table S1). Primers used for cloning and mutagenesis are listed in Supplementary Table S1B.

IFN exposure of melanoma cell cultures

A total of 24 hours after seeding 1×10^6 melanoma cells in a 10 cm plate, cell media was substituted with 10 mL of media with and without 10 ng/mL of human recombinant IFN γ protein (R&D Systems, catalog no. 285-IF) or 1,000 IU/mL of recombinant IFN- α 2a protein (Roferon-A, Roche). A total of 48 hours following IFN exposure, cells were collected for flow cytometry (FACS) analysis as described below, and the remaining cells were pelleted and frozen for RNA and protein extraction as indicated below. The IFN γ responsiveness score was calculated by averaging the fold changes of two genes (*HLA-B* and *IFIH1*) and two proteins [PD-L1 and phosphorylated (p)STAT1], which were significantly altered between MYC and Mock-overexpressing cells following IFN γ exposure (1.5-fold decrease in expression and $P < 0.05$ in at least two cell lines).

Flow cytometry

After harvesting, 1×10^5 Mock and MYC overexpression melanoma cells were transferred to a 96-well U-shaped plate. Flow cytometry staining was performed with the appropriate antibodies (Supplementary Table S1A) diluted in FACS medium [PBS, 0.02% sodium azide (Bioworld, catalog no. 40120990), and 0.5% BSA (MP Biomedicals catalog no. 0216006980)] on ice for 30 minutes. For controls, we used appropriate isotype controls for conjugated antibodies or secondary antibodies only for unconjugated antibodies. Following incubation, cells were centrifuged (5 minutes, $500 \times g$, 4°C), washed, and resuspended in 200 μ L FACS medium and collected for FACS analysis. All experiments were performed using a MACSquant Analyzer 10 Flow Cytometer (Miltenyi Biotec), and data analysis was conducted in the Kaluza software (Beckman Coulter Life Sciences).

RNA extraction, cDNA preparation, and qRT-PCR

RNA was extracted from cultured melanoma cells using TRI Reagent (Sigma-Aldrich, catalog no. T9424) according to manufacturer protocol. cDNA was generated by the qScript cDNA Synthesis Kit (Quantabio, catalog no. 95047). Forward and reverse primers were designed from different exons to eliminate possible DNA contamination. Gene transcripts were detected using PerfeCTa SYBR Green FastMix (Quantabio, catalog no. 95071). The qRT-PCR reactions were run in triplicates of 20 ng RNA in 10 μ L per well, on a StepOnePlus Real-Time PCR system (Applied Biosystems). Reactions were normalized to the 18S endogenous control. Relative expression was calculated using $2^{-\Delta\Delta C_t}$ equation. The detailed list of primers used for qRT-PCR is in Supplementary Table S1C.

Protein extraction and Western blot analysis

Cultured Mock and MYC overexpression melanoma cells were washed with PBS and lysed in RIPA lysis buffer (Bioworld, catalog no. 42020032-2), DNase (MERCK, catalog no. 69182), and phosphatase and protease inhibitor cocktail (Bimake, catalog nos. 14001 and 15001) on ice for 20 minutes. Insoluble material was removed by centrifugation at 14,000 rpm for 20 minutes at 4°C. Protein concentration was measured using Pierce BCA protein kit (Thermo Fisher Scientific, catalog no. 23225). A total of 50 μ g of protein was loaded and separated by 6%–15% SDS-PAGE, transferred onto nitrocellulose membranes (Bio-Rad, catalog no. 1704159), and incubated with specific antibodies (Supplementary Table S1A). The antigen-antibody complexes were visualized by a standard enhanced chemiluminescence detection kit for horseradish peroxidase (Biological-Industries, catalog no. 20-500-1000). Densitometry with ImageJ (NIH) was used for protein quantification.

Luciferase reporter assay

The JAK2 promoter sequence (NM_001233195, –1,000 to +100 bps from transcription start site) was amplified using a thermocycler (Applied Biosystems 2720 Thermal Cycler, Thermo Fisher Scientific, catalog no. 4359659) and cloned using the Gibson Assembly Master Mix (New England Biolabs, catalog no. E2611) into pGL4.14 vector (Promega), downstream of the Firefly luciferase gene. After identification of three MYC binding sites in the JAK2 promoter using the Eukaryotic Promoter Database (34), the three MYC binding sites were mutated by replacing the Cytosine (C) base with adenine (A) using KOD Hot Start DNA Polymerase (MERCK, catalog no. 71086). To measure the effect of MYC overexpression on JAK2 promoter activity, Firefly luciferase reporter vectors under the control of wildtype or mutant JAK2 promoter were cotransfected with a pRL-TK *Renilla* luciferase control reporter vector (Promega, catalog no. E2241) into MYC and Mock-overexpressing melanoma cells in a 1:10 ratio using jetPRIME transfection reagent (Polyplus, catalog no. 114) according to manufacturer's instructions. After 24 hours, cells were lysed using passive lysis buffer (Promega, catalog no. E1941), and luciferase activity was measured using a Dual Luciferase Reporter Assay System (Promega, catalog no. 1960) in a GlowMax microplate reader (Promega) and normalized to the *Renilla* signal.

MYC and MAX silencing by siRNA

A total of 24 hours after seeding 2.5×10^5 melanoma cells in a 6-well plate, cells were transfected with 20 nmol/L of MYC (Dharmacon, catalog no. L-003282-02) or MAX (Dharmacon, catalog no. L-010092-00) ON-TARGETplus SMARTpool siRNA or scrambled sequence siRNA using the jetPRIME transfection reagent (Polyplus, catalog no. 114) according to manufacturer's instructions. After incubation at 37°C overnight, the transfected melanoma cells were washed and recultured with fresh RPMI1640 based media. Gene silencing was validated by qRT-PCR and Western blot analysis.

IFN γ secretion via ELISA

MYC or Mock-overexpressing melanoma cells transfected with either MAX or control siRNA were coincubated with autologous TILs in a 2.5:1 effector to target cell ratio for 18 hours. Following incubation, 50 μ L of supernatant was collected from each sample and the amount of IFN γ was evaluated by a standardized ELISA (BioLegend, catalog no. 430104) according to manufacturer's instructions. Absorbance was measured using Glowmax plate reader (Promega).

CD137 (4-1BB) upregulation assay

MYC or Mock-overexpressing melanoma cells were coincubated with autologous TILs in a 2.5:1 effector to target cell ratio for 18 hours to measure CD137 expression. Following incubation, TILs were collected and CD8⁺ T cells were analyzed for CD137 expression by flow cytometry using CD8a (BioLegend, catalog no. 301008) and CD137 (BioLegend, catalog no. 309810) antibodies.

TIL degranulation assay

MYC or Mock-overexpressing melanoma cells were coincubated with autologous TILs in a 2.5:1 effector to target cell ratio for a total of 6 hours with CD107a antibody (BioLegend, catalog no.328607). After 1 hour of incubation, Monensin A solution (BioLegend, catalog no. 420701) was added to the culture for an additional 5 hours. Following incubation, the cells were stained with CD8 antibody (BioLegend, catalog no. 344721) to measure the CD8⁺CD107a⁺ population and CD107a mean fluorescence intensity by flow cytometry. Degranulation was assessed by comparison

with base line CD107a expression of TILs which were not incubated with melanoma cells.

Ruxolitinib exposure of melanoma cell cultures

A total of 24 hours after seeding 3×10^5 melanoma cells in a 6-well plate, cell media was substituted with 3 mL of media with and without 30 $\mu\text{mol/L}$ of the JAK inhibitor ruxolitinib (Selleckchem, catalog no. S1378). A total of 24 hours following ruxolitinib exposure, cells were collected and coincubated with autologous TILs in a 2.5:1 effector to target cell ratio for 18 hours to measure IFN γ secretion as described above.

Statistical analysis

The R software (version 4.0.3) was used for statistical analysis and visualization. Unless mentioned otherwise, the statistical test used for continuous variables was the unpaired two-tailed Welch *t* test, whereas categorical variables were analyzed using Fisher exact test. Correction for multiple testing was made with the Benjamini–Hochberg procedure. Differential gene expression analysis was according to the LIMMA R package pipeline. Correlation analysis was performed using the Pearson correlation coefficient. For pathway enrichment analysis, annotated gene sets were downloaded from the Molecular Signatures Database. Identification of overrepresented or underrepresented pathways in a subgroup of genes was performed using the hypergeometric test. Identification of over or underrepresented pathways in a ranked gene list was performed using the GSEA algorithm (27). Kaplan–Meier plots were generated using the survival and survminer R packages. When implementing survival analysis on gene list scores, we compared the upper and lower medians, unless mentioned otherwise. *P* values for survival analyses were computed using the log-rank test.

Code and data availability

RNA-seq data were uploaded to the NCBI GEO (GSE160638). All other data supporting the findings of this study will be available from the corresponding authors upon reasonable request.

Results

Assembly of preimmunotherapy patient cohort

In a recent article by Harel and colleagues, we profiled the pre-treatment proteomes of responders and nonresponders to TIL ACT and PD-1 blockade in patients with advanced melanoma (17). We identified a link between oxidative metabolism and upregulation of the antigen processing and presentation machinery in responders to immunotherapy, whereas in the proteomic analysis, we focused on melanoma-intrinsic pathways associated with immunotherapy outcome. Here, we integrated the proteomic findings with RNA-seq from the same tumor biopsies. Thus, we further deepened our biological and clinical findings from the proteomic analysis and obtained a more accurate description of low abundance genes such as cytokines and immune-related transcriptional networks. These are also of importance to our understanding of the underlying mechanisms of response and resistance to immunotherapy (14, 22). In total, we assembled a cohort of 73 preimmunotherapy tumor biopsies from patients treated with either TIL ACT ($n = 37$) or PD-1 blockade ($n = 36$) with available transcriptomic and proteomic data (patient characteristics in Supplementary Table S2A). All of the TIL ACT–treated patients were PD-1 blockade naïve, and in both TIL ACT and PD-1 blockade cohorts, prior treatments with ipilimumab or MAPK inhibitors did not significantly alter the response to either treatment, although the number of previously treated patients was low (Supplementary Table S2B and S2C).

The two main clinical differences between the TIL ACT and PD-1 blockade cohorts were the age at treatment initiation (53.4 vs. 60.7, $P = 0.02$) and the number of previous treatments (1.6 vs. 0.5, $P < 0.001$; Supplementary Table S2D). These differences can be attributed to the fact that TIL ACT requires lymphodepletion with high-dose chemotherapy and thus it is less suitable for older patients, and that it is still an experimental treatment given only after failure of standard-of-care treatments. Male gender and normal plasma lactate dehydrogenase were associated with higher response rate in the TIL ACT cohort as was reported previously (ref. 17; Supplementary Table S2B).

Transcriptome profiling of responders and nonresponders to immunotherapy

After RNA-seq, alignment and filtration of lowly expressed genes and lowly detected proteins, we quantified 17,000 genes and 7,300 proteins that were expressed in both cohorts. To evaluate the relationship between expression and detection probability in the proteomics data, the average TPM of each gene was plotted by the percent detection in the proteomics data. In agreement with previous articles (35, 36), we observed a detection bias toward more abundant genes in the proteomic data (Supplementary Fig. S1A), as was reflected by a 3-fold increase in the detection probability of abundant genes (above the median of the average TPM values) compared with genes below the median of the average TPM values (60.5% vs. 19.3% detection probability, Fisher exact test, $P < 0.0001$). Pathway enrichment analysis demonstrated overrepresentation of pathways related to cell homeostasis in the detected proteins, such as spliceosome-, proteasome-, ribosome-, metabolism-, and DNA replication-related pathways (Supplementary Fig. S1B; Supplementary Table S3A). This was accompanied by underrepresentation of pathways related to signal transduction and immune activation, such as cytokine, hedgehog, JAK-STAT, and TGF β signaling pathways (Supplementary Fig. S1B; Supplementary Table S3B). Because the proteomic data focused mainly on melanoma-intrinsic proteins, we indeed observed a high detection probability of melanoma cell markers compared with immune cell markers (77% vs. 49.5%, Fisher exact test, $P < 0.0001$; Supplementary Fig. S1C). In the transcriptomic data, we quantified more than 95% of melanoma, stroma, and immune cell markers. Thus, RNA-seq was complementary to our proteomic profiling, and the increased depth of coverage allowed us to better assess immune-related and lowly expressed genes such as cytokines, signal transduction molecules, and immune cell activation markers.

One of the main advantages of profiling both the transcriptome and proteome from the same tumor biopsies is the ability to assess the dependence between mRNA expression and protein levels. We observed a weak correlation between mRNA expression and protein levels on the gene level (median Person $r = 0.25$; Supplementary Table S3C). However, we found that the proteins exhibiting a high correlation between mRNA and protein levels (Pearson r above upper quartile) were enriched for processes such as epithelial–mesenchymal transition, hypoxia, and IFN signaling, whereas proteins with low correlation (Pearson r below lower quartile) were enriched for cell homeostasis processes such oxidative phosphorylation and DNA repair (Supplementary Tables S3D and S3E). These findings agree with a recent article that demonstrates that homeostatic cellular functions are predominantly regulated posttranscriptionally and that induced cellular functions, such as signal transduction and immune activation, are driven through transcriptional regulation (37).

To identify the sources of intersample variability in our transcriptomic data, we performed principal component analysis on the 3,000 most variable genes (Supplementary Fig. S1D). The first primary

component (PC1) was significantly correlated with the extent of tumor immune infiltration as assessed by the ImmuneScore ($r_p = 0.98$, $P < 0.0001$; Supplementary Fig. S1E), a method based on gene expression signatures to infer the fraction of immune cells in tumor samples (26). The gene that was most highly correlated with the second primary component was with the microphthalmia-associated transcription factor *MITF* ($r_p = 0.87$, $P < 0.0001$; Supplementary Fig. S1E), a key transcription factor for melanocyte development, differentiation, and survival (38). Hence, the two main sources of intersample variation were the extent of tumor immune infiltration and the degree of differentiation of the melanoma cells.

In agreement with Harel and colleagues, we found that the transcriptomic features associated with response and resistance to TIL ACT and PD-1 blockade were very similar (Supplementary Fig. S1F and S1G). When comparing the transcriptome of responders and nonresponders to TIL ACT, we did not find DEGs below the adjusted P -value cutoff (moderated t test, FDR < 0.05 ; Supplementary Table S4A); however, we identified 1,048 differentially expressed genes in the PD-1 blockade cohort (moderated t test, FDR < 0.05 ; Supplementary Table S4B). We identified a strong correlation between the \log_2 fold change of the top 500 DEGs in each cohort ($r_p = 0.74$, $P < 0.0001$; Supplementary Fig. S1F), as well as a strong correlation between the GSEA (27) normalized enrichment scores ($r_p = 0.84$, $P < 0.0001$; Supplementary Fig. S1G) of differentially expressed Hallmark gene sets (FDR < 0.05 ; Supplementary Table S4C and S4D; ref. 28).

Because of the similarities in response and resistance pathways to TIL ACT and PD-1 blockade, we conducted a joint analysis to identify global response and resistance mechanisms to immunotherapy. Transcriptome comparison between responders and nonresponders to both treatments identified 2,150 DEGs (moderated t test, FDR < 0.05 ; Fig. 1A; Supplementary Table S5A). Hierarchical clustering of samples according to expression of DEGs enabled us to divide the patients into three distinct clusters, Immune high, med, and low, which differed in the extent of tumor immune infiltration as assessed by the ImmuneScore (Fig. 1B) and clinical outcome (Fig. 1C). Whereas patients in the Immune high cluster had 95% overall response rate, patients in the Immune low cluster had only 9% response rate (Fisher exact test, $P < 0.0001$). To examine whether the abundance of particular cell types associated with response to immunotherapy, we used xCell, a gene signature-based method for inference of the tumor immune and stromal cell composition (29). In accordance with previous reports (10, 14, 16), we did not find a single cell type whose estimated abundance associated with response to immunotherapy, but rather a milieu of immune cells, most notably B cells, T cells, and dendritic cells (Fig. 1D; Supplementary Table S5B).

Hierarchical clustering of the 2,150 DEGs resulted in three distinct gene clusters (Fig. 1A; Supplementary Table S5C). Gene Ontology enrichment analysis for upregulated genes in nonresponders (Cluster 3 genes) demonstrated overrepresentation of oncogenic pathways such as cell cycle and dedifferentiation (Supplementary Table S5D), whereas gene clusters which were upregulated in responders (Cluster 1 and Cluster 2 genes) were enriched for immune-related pathways such as immune effector process and IFN response genes (Supplementary Table S5E and S5F). Although Cluster 1 genes were predominantly enriched for innate immunity-related pathways such as myeloid activation, Cluster 2 genes were enriched for adaptive immunity-related pathways such as lymphocyte activation. Distribution of cluster genes in each cell type in a melanoma scRNA-seq dataset (16, 25) demonstrated that Cluster 2 genes were expressed mostly within

immune cells and Cluster 1 genes were relatively equally distributed within all cell types, including melanoma cells (Fig. 1G). In accordance, Cluster 2 genes highly correlated with the ImmuneScore ($r_p = 0.95$, $P < 0.0001$; Fig. 1F) and contained numerous Lymphocyte marker genes such as T-cell markers (CD3 and CD8) and B-cell markers (CD19 and CD20). Thus, we concluded that Cluster 2 genes (“Lymphocyte markers”) represent lymphocyte infiltration and activation within tumors. Distribution of gene cluster scores, calculated by GSVA (30), demonstrated a strong inverse correlation between Cluster 1 and Cluster 3, both in our immunotherapy cohort ($r_p = -0.95$, $P < 0.0001$; Fig. 1E) and in a combined cohort of melanoma RNA-seq datasets ($n = 356$) comprised of metastatic samples from TCGA SKCM dataset and previously published immunotherapy pretreatment RNA-seq datasets of patients with melanoma which were treated with either PD-1 blockade or TIL ACT (refs. 10, 12, 22–24; $r_p = -0.89$, $P < 0.0001$; Supplementary Fig. S2B). Cluster score distribution by cell type in a melanoma scRNA dataset demonstrated a strong inverse correlation between Cluster 1 and Cluster 3, most prominently within melanoma cells ($r_p = -0.89$, $P < 0.0001$; Fig. 1H) and cancer-associated fibroblasts ($r_p = -0.78$, $P < 0.0001$; Supplementary Fig. S2A). Melanoma cells from tumors that progressed on PD-1 blockade exhibited higher Cluster 3 scores, as well as lower Cluster 1 scores, compared with anti-PD-1-naïve melanomas (Welch t test, $P < 0.0001$; Fig. 1G and H; Supplementary Fig. S2C). Thus, we concluded that Cluster 1 (“Melanoma response”) and Cluster 3 (“Melanoma resistance”) represent two mutually exclusive and melanoma-intrinsic cell programs, which determine immunotherapy responsiveness and resistance.

To assess the effect of the melanoma-intrinsic immunotherapy resistance and response programs on treatment outcome, we compiled the MIRScore by subtracting the Melanoma response cluster score from the Melanoma resistance cluster score. Although previous reports have identified immune cell infiltration as the main predictor for immunotherapy outcome (14, 39), we found that compared with tumor immune cell infiltration, as assessed by ImmuneScore or the Lymphocyte marker gene cluster score, the MIRScore exhibited comparable or better performance as a predictor for overall survival following immunotherapy (Fig. 1I; Supplementary Fig. S2D and S2E). This finding was observed both in our immunotherapy cohort at the mRNA (Fig. 1I) and protein levels (Supplementary Fig. S2D) and in the combined cohort of previously published melanoma RNA-seq datasets (Supplementary Fig. S2E).

Finally, although we previously observed an upregulation of oxidative metabolism in the proteomes of responders to immunotherapy (17), we did not observe an enrichment for oxidative metabolism gene sets in the transcriptomes of the same patients. As mentioned above, we detected an enrichment for oxidative phosphorylation proteins in genes with low correlation between mRNA and protein levels, thus suggesting that oxidative metabolism is regulated posttranscriptionally.

MYC and IFN γ are regulators of the Melanoma resistance and response cell programs

To better characterize the melanoma-intrinsic immunotherapy response and resistance cell states, we compiled a combined melanoma dataset ($n = 403$), comprised of seven melanoma RNA-seq datasets with available raw counts—our TIL ACT ($n = 37$) and PD-1 blockade ($n = 36$) cohorts, metastatic samples from TCGA SKCM dataset ($n = 68$), and four previously published PD-1 blockade datasets: Hugo and colleagues ($n = 27$), Riaz and colleagues ($n = 47$), Gide and colleagues ($n = 73$), and Liu and colleagues ($n = 115$; refs. 10, 12, 22, 24).

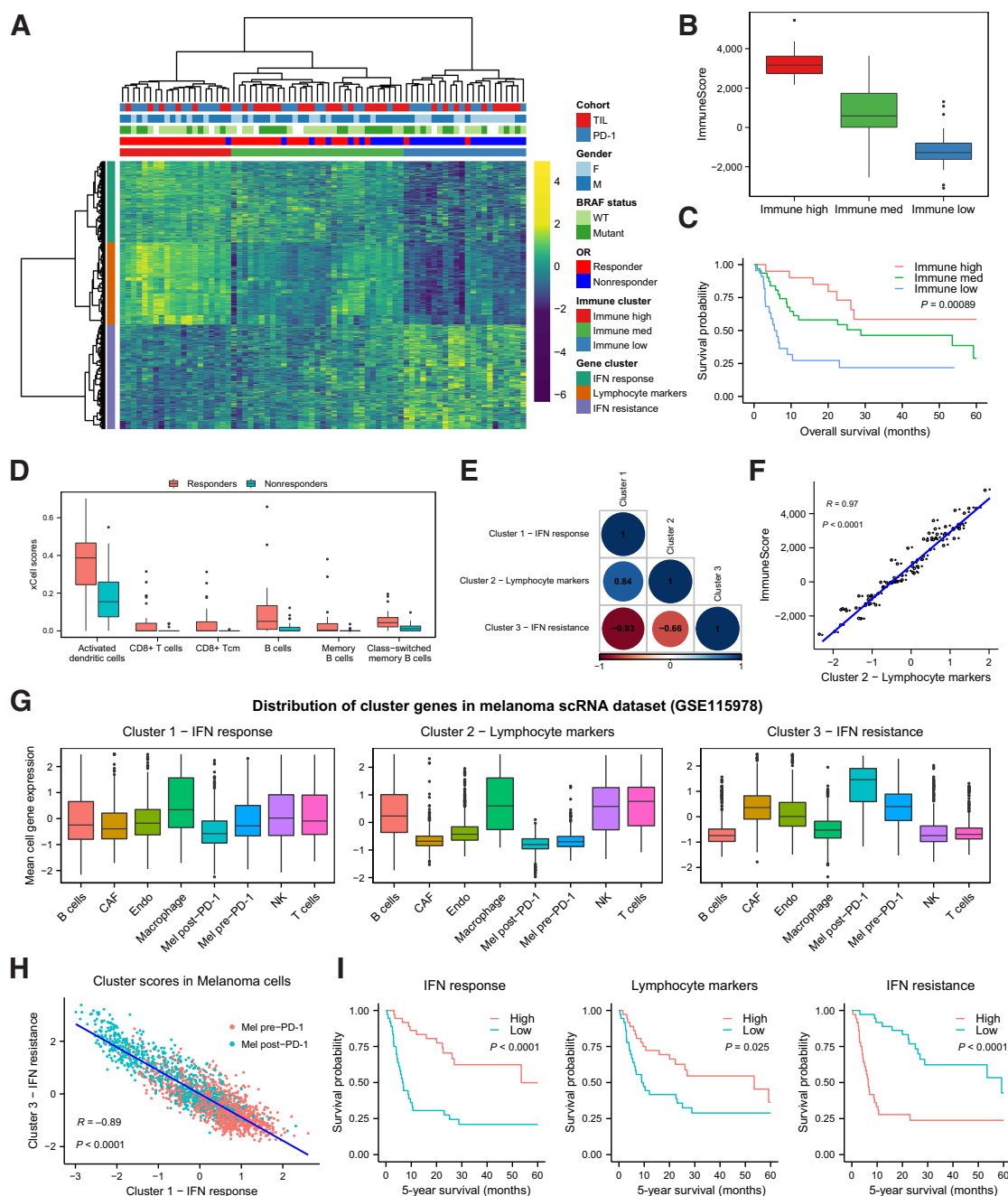


Figure 1.

Transcriptome profiling of responders and nonresponders to immunotherapy. The transcriptome of responders ($n = 41$) and nonresponders ($n = 32$) to TIL ACT and PD-1 blockade was assessed via RNA-seq. **A**, Hierarchical clustering of 2,150 differentially expressed genes (moderated t test, FDR < 0.05) between responders and nonresponders to immunotherapy and identification of three main DEG clusters and three main immune clusters of patients. See also Supplementary Table S5A and S5C. The ImmuneScore (**B**) and 5-year survival (**C**) of patients in the Immune high ($n = 20$), med ($n = 31$), and low ($n = 22$) clusters. **D**, xCell scores of immune cells which were differentially distributed between responders ($n = 41$) and nonresponders ($n = 32$) to immunotherapy (Wilcoxon rank-sum test, FDR < 0.05). See also Supplementary Table S5B. **E**, Pearson correlation between the three cluster scores. **F**, Pearson correlation between the Lymphocyte marker cluster score and the ImmuneScore. **G**, Distribution of cluster gene mean expression in a melanoma scRNA-seq dataset (GSE115978). CAF, cancer-associated fibroblasts; Endo, endothelial cells. **H**, Pearson correlation between the Melanoma response and resistance cluster scores in PD-1 blockade-naïve (pre-PD1) and resistant (post-PD1) melanoma cells (GSE115978). **I**, Comparison of 5-year survival between patients with high (above median, $n = 36$) and low (below median, $n = 36$) MIRScore, computed by subtracting the Melanoma response cluster score from the Melanoma resistance cluster score, Lymphocyte marker cluster score, and the ImmuneScore in our immunotherapy cohort. P values for survival analyses were computed using the log-rank test. For the box plots in **B**, **D**, and **G**, the horizontal lines within each box denote median values, the bottom and top edges of the box represent the 25th and 75th percentiles, and the whiskers extend to the lowest and highest datapoints within 1.5 times the interquartile range from the edge of the box.

Transcriptome comparison between tumors with high MIRScore (upper third, $n = 134$) and low MIRScore (lower third, $n = 135$) in the combined melanoma dataset resulted in more than 7,800 DEGs (moderated t test, FDR < 0.05; Supplementary Table S6A). Hierarchical clustering of the top 1,000 DEGs demonstrated segregation into three main clusters, which were strongly correlated with the previously identified Melanoma response, Leukocyte markers, and Melanoma resistance gene clusters (Fig. 2A; Supplementary Fig. S3A; Supplementary Table S6B). Pathway enrichment analysis of the Molecular Signature Database–curated and Hallmark gene sets identified “Cairo hepatoblastoma classes up” as the most overrepresented gene set in the new Melanoma resistance cluster (Supplementary Table S6C). This gene set represents genes that are upregulated in a highly proliferative and dedifferentiated subclass of hepatoblastoma, characterized by upregulation of MYC signaling (40). The top two enriched Hallmark gene sets were MYC target genes (Supplementary Table S6D). In the new Melanoma response cluster, the most overrepresented gene sets were genes that were upregulated upon EZH2 knockdown and IFN response genes (Supplementary Table S6E and S6F). EZH2, a histone methyltransferase, which is the functional enzymatic component of the Polycomb Repressive Complex 2, is upregulated by MYC and can induce immunotherapy resistance by repression of the antigen processing and presentation pathway in melanoma cells (41, 42). Because both of the top overrepresented pathways in the Melanoma resistance and response clusters associated with MYC activation and inhibition, we recognized MYC as a potential facilitator of the melanoma resistance phenotype. Further corroborating this assumption, Ingenuity upstream regulator analysis in ingenuity pathway analysis (IPA) identified MYC as the top upstream regulator associated with the Melanoma resistance phenotype (activation Z-score = 6.2, $P < 0.0001$), whereas IFN γ was the top upstream regulator associated with the Melanoma response phenotype (activation Z-score = -9.8, $P < 0.0001$; Fig. 2B). Comparison of MYC mRNA expression between the three patients’ clusters demonstrated upregulation of MYC mRNA in the Immune low group ($P = 0.03$, Welch t test; Supplementary Fig. S3B). We further observed an upregulation of MYC activity in pretreatment biopsies from nonresponding patients to PD-1 blockade, demonstrated by a 4-fold increase in high MYC nuclear stain [41.2% ($n = 18$) vs. 11.1% ($n = 17$), Fisher exact test, $P = 0.06$; Fig. 2C] and overrepresentation of MYC target genes in transcriptomes of nonresponders ($n = 14$) versus responders ($n = 22$) to PD-1 blockade ($P < 0.01$, Welch t test, Fig. 2D), as assessed by GSVA (30). No significant difference in high MYC cytoplasmic stain was observed between responders and nonresponders (38.9% vs. 17.6%, Fisher exact test, $P = 0.26$). Comparison between protein expression of MIRScore^{high} (upper third, $n = 117$) and MIRScore^{low} (lower third, $n = 117$) tumors in TCGA SKCM cohort revealed that MYC was among the most significantly upregulated proteins in MIRScore^{high} tumors (Fig. 2E; Supplementary Table S6G). Taken together, we suggest that the Melanoma response and resistance cell programs are regulated by the opposing functions of IFN γ and MYC, which dictate immunotherapy outcome.

To assess whether the MYC and IFN γ controlled Melanoma response and resistance clusters reflected mutually exclusive cell programs in other malignancies, we measured the correlation between the two cluster scores in RNA-seq data from 32 cancer types in TCGA (Supplementary Table S6H). Indeed, the Melanoma response and resistance clusters inversely correlated ($r_p < -0.45$, $P < 0.0001$) in all cancer types (Supplementary Fig. S3C). Thus, we suggest that there is a strong inverse correlation between MYC and IFN γ activity across a broad spectrum of tumors.

MYC overexpression induces IFN γ resistance through JAK2 downregulation

Several articles report that IFN signaling can inhibit MYC expression through both downregulation of MYC mRNA and increased proteasomal degradation (43, 44). Therefore, it is unclear whether the overrepresentation of MYC target genes in the Melanoma response cluster, which is regulated by IFN γ , is causal (due to a direct inhibitory effect of MYC on IFN signaling) or circumstantial (a lack of IFN signaling prevents MYC inhibition in *a priori* IFN-resistant tumors). To answer this question, stably transfected cells with MYC and Mock overexpression vectors from patient-derived melanoma cell cultures (Supplementary Fig. S4A) were exposed to IFN γ for 48 hours. Following IFN γ exposure, all Mock transfected cell lines were responsive to IFN γ , as exhibited by upregulation in seven IFN γ -stimulated genes (*B2M*, *HLA-B*, *IFIH1*, *IRF1*, *JAK2*, *PARP9*, and *STAT1*), PD-L1 protein expression, and IFN γ -mediated phosphorylation of STAT1 at Y701 (pSTAT1), the downstream effector of IFN γ signaling (Supplementary Fig. S4B–S4D). MYC overexpression did not significantly affect IFN γ responsiveness in cells from an Immune high responder to TIL ACT (Mel 111) and a patient-derived melanoma cell line (Mel 526). In contrast, MYC-overexpressing cells from Immune low nonresponders to TIL ACT (Mel 53, 90, and 131) demonstrated a significant reduction in IFN γ responsiveness, as reflected by a decrease both induction and expression of IFN γ -stimulated genes, PD-L1 expression, and pSTAT1 following IFN γ exposure (Fig. 3A–C; Supplementary Fig. S4E and S4F).

To assess the level of MYC-induced IFN γ resistance, we constructed an IFN γ responsiveness score by averaging the fold changes of two genes (*HLA-B* and *IFIH1*) and two proteins (PD-L1 and pSTAT1) that were significantly altered following IFN γ exposure between MYC and Mock-overexpressing cells in at least two cell lines (Fig. 3D). Indeed, the IFN γ responsiveness score showed a spectrum of MYC-induced IFN γ resistance, with the greatest effect in the immune low TIL ACT-resistant melanomas and almost no effect in the Immune high TIL ACT-responsive melanoma cell line (Fig. 3D). Hence, MYC upregulation can induce IFN γ resistance in predisposed tumors.

The IFN γ signaling pathway is initiated by the binding of IFN γ to its receptor, a heterodimer of the IFNGR1 and IFNGR2 chains, followed by phosphorylation of JAK1, JAK2, and STAT1 (45). In light of the decrease in IFN γ -induced pSTAT1 in MYC-overexpressing cells after IFN γ exposure, we speculated that MYC affected IFN γ signaling upstream of STAT1 Y701 phosphorylation. To address this hypothesis, we mapped the mRNA and protein expression of the IFN γ signaling pathway upstream of pSTAT1 in both MYC and Mock-overexpressing cell lines. MYC overexpression significantly reduced JAK2 mRNA and protein expression in all of the Immune low melanoma cell lines, but not in Mel 111 and Mel 526 (Fig. 4A–C; Supplementary Fig. S5A and S5B). MYC target genes were the most significantly enriched Hallmark pathway (hypergeometric test, FDR < 0.0001) in genes which were strongly inversely correlated ($r_p < -0.6$) with JAK2 mRNA in the combined melanoma dataset ($n = 403$; Supplementary Fig. S5C). Because JAK2 mutations are shown to induce acquired resistance to PD-1 blockade (13), we speculated that MYC induced immunotherapy resistance by JAK2 downregulation. JAK2 was the only member of the IFN γ signaling pathway that had a significant correlation between its fold reduction in MYC-overexpressing cells and the IFN γ responsiveness score ($r_p = 0.93$, $P = 0.02$; Fig. 4D), suggesting that indeed the mechanism by which MYC confers IFN γ resistance is through JAK2 downregulation.

Phosphorylation of STAT1 also occurs following IFN α signaling. However, although JAK2 is essential for IFN γ signaling, it is not

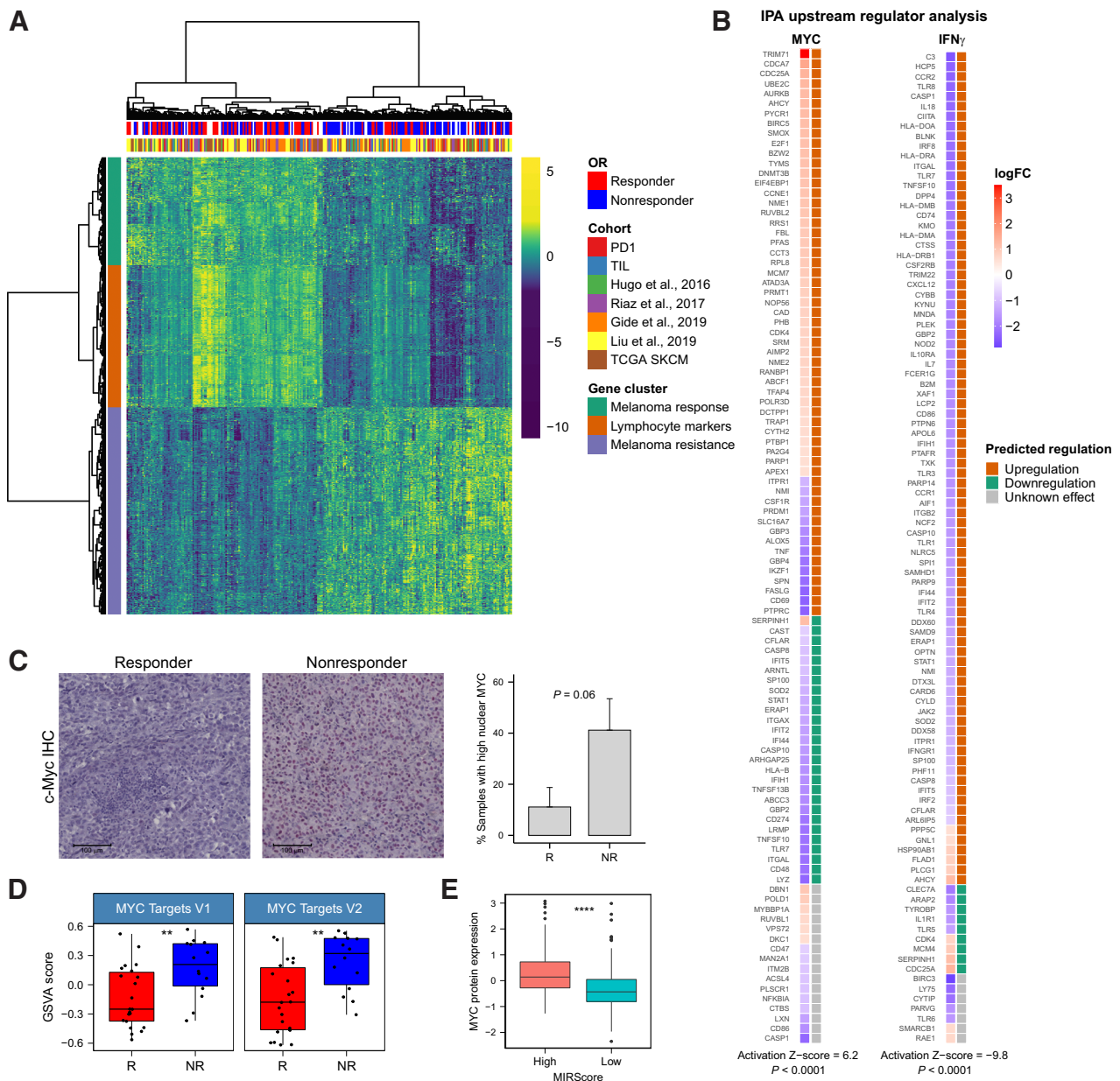


Figure 2.

c-Myc and IFN γ are regulators of the Melanoma resistance and response cell programs. **A**, Hierarchical clustering of the top 1,000 DEGs between MIRScore high (upper third, $n = 134$) and low (lower third, $n = 135$) tumors in seven combined melanoma RNA-seq datasets with available raw counts—our TIL ACT and PD-1 blockade datasets, four previously published PD-1 blockade datasets (GSE78220, GSE91061, PRJEB23709, and phs000452.v3.p1; refs. 10, 12, 22, 24) and metastatic samples from TCGA SKCM dataset. See also Supplementary Table S6A and S6B. **B**, IPA upstream regulator analysis of DEGs between MIRScore^{high} and MIRScore^{low} tumors, whereas the right column represents the expected regulatory effect of each transcription regulator as stored in the Ingenuity Knowledge Base. **C**, Right: The percent of samples with high nuclear MYC stain in a tumor microarray (TMA) of pretreatment biopsies from responders (R, $n = 18$) and nonresponders (NR, $n = 17$) to PD-1 blockade. Left: Representative 0.5 mm² images of MYC staining in a responder and nonresponder to PD-1 blockade from the TMA. **D**, MYC activity, as assessed by GSVAs of Hallmark MYC targets gene sets, in transcriptomes of responders (R, $n = 22$) and nonresponders (NR, $n = 14$) to PD-1 blockade. **E**, Protein expression of MYC in MIRScore^{high} (upper third, $n = 117$) and MIRScore^{low} (lower third, $n = 117$) tumors, as assessed by RPPA from TCGA SKCM dataset. See also Supplementary Table S6G. *P* values in **C–E** were calculated using Welch *t* test. *, $P < 0.05$; **, $P < 0.01$; ***, $P < 0.001$; ****, $P < 0.0001$. Bar plot data are represented as mean + SEM. For the box plots in **C** and **D**, the horizontal lines within each box denote median values, the bottom and top edges of the box represent the 25th and 75th percentiles, and the whiskers extend to the lowest and highest data points within 1.5 times the interquartile range from the edge of the box.

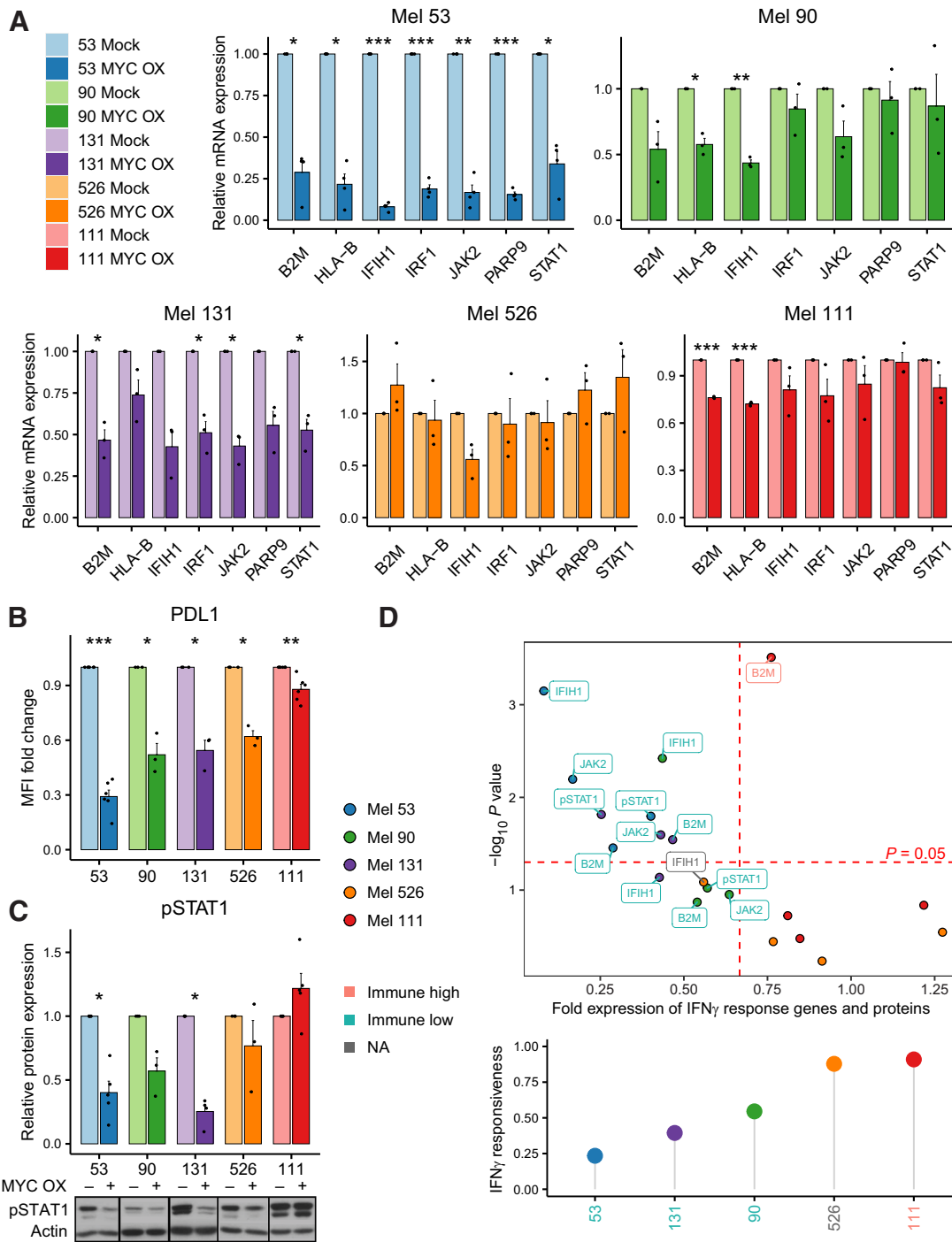


Figure 3. MYC overexpression induces IFN γ resistance in patient-derived melanoma cell lines. Patient-derived melanoma cell cultures were stably transfected with MYC or Mock overexpression vectors, followed by exposure to 10 ng/mL of recombinant IFN γ for 48 hours. **A** and **B**, Relative mRNA expression of seven IFN γ -stimulated genes via qRT-PCR (**A**) and PD-L1 median fluorescence intensity via flow cytometry (**B**) between MYC and Mock-overexpressing cells. **C**, Top: Western blots were used to assess IFN γ -induced STAT1 phosphorylation (pSTAT1) in cells with and without MYC overexpression, as assessed by immunoblot densitometry. Bottom: Representative immunoblots of pSTAT1. Each individual experiment is delineated. **D**, Top: Visualization of fold changes and *P* values of IFN γ response genes (HLA-B and IFIH1) and proteins (PD-L1 and pSTAT1) significantly altered between MYC and Mock-overexpressing cells following IFN γ exposure (1.5-fold decrease in expression and *P* < 0.05 in at least two cell lines). Label colors represent the immune cluster of the tumor from which the melanoma cell lines were derived (unknown for Mel 526, see Fig. 1A and B). NA, nonapplicable. Bottom: The IFN γ responsiveness score for each MYC-overexpressing melanoma cell line, as calculated by the mean fold change of the four significantly altered IFN γ response genes and proteins. Bar plot data are represented as mean + SEM, where each dot signifies a single experiment. *P* values in **A–C** were computed using a paired *t* test. *, *P* < 0.05; **, *P* < 0.01; ***, *P* < 0.001.

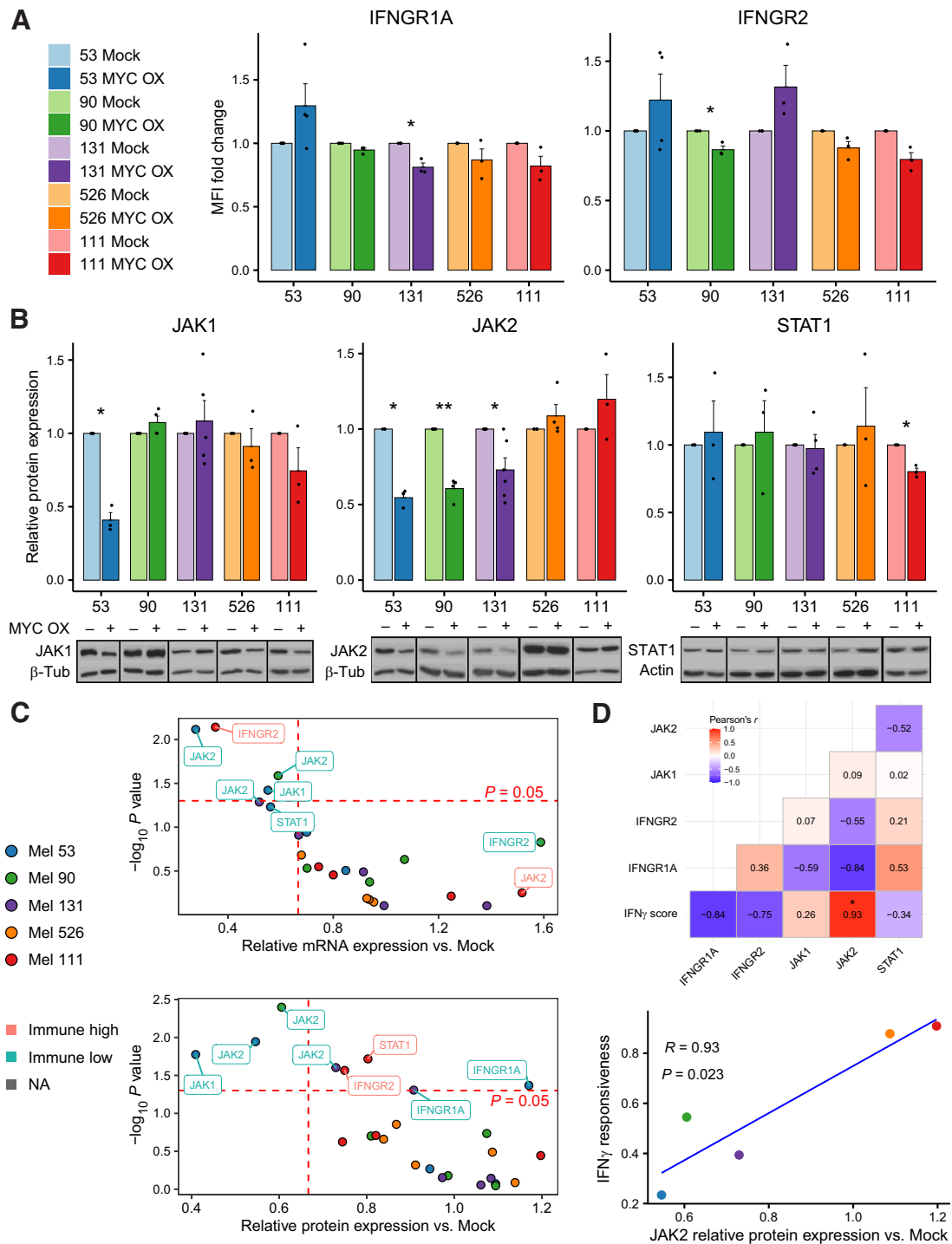


Figure 4.

MYC-induced IFN γ resistance is associated with JAK2 downregulation. The expression of the IFN γ signaling pathway components in MYC and Mock stably transfected cell from patient-derived melanoma cell lines was determined. **A**, Relative median fluorescence intensity (MFI) via flow cytometry of IFN γ receptor chains IFNGR1 and IFNGR2 between MYC and Mock-overexpressing cells. **B**, Top: Relative protein expression, as assessed by immunoblot densitometry, of the intracellular components of the IFN γ signaling pathway. Bottom: Representative immunoblots of the IFN γ signaling proteins. Each individual experiment is delineated. **C**, Visualization of fold changes and P values of the IFN γ signaling genes (top) and proteins (bottom) between MYC and Mock-overexpressing cells. Label colors represent the immune cluster of the tumor from which the melanoma cell lines were derived (unknown for Mel 526, see **Fig. 1A** and **B**). NA, Nonapplicable. **D**, Top: Correlation matrix between the relative protein expression of the IFN γ signaling pathway components in MYC-overexpressing cells versus Mock and the IFN γ responsiveness score (IFN γ score) as calculated in **Fig. 3D**. Bottom: JAK2 relative expression in MYC-overexpressing cells versus mock. Bar plot data are represented as mean + SE, where each dot represents a single experiment. P values in **A** and **B** were computed using a paired t test. *, $P < 0.05$; **, $P < 0.01$; ***, $P < 0.001$.

required for IFN α signaling, as STAT1 and STAT2 phosphorylation occurs through JAK1 and TYK2 signaling (46). Therefore, we investigated whether IFN α signaling was hindered in the Immune low cell lines in addition to IFN γ signaling. We did not observe a significant reduction in IFN α responsiveness, as reflected by similar expression and induction of three IFN α -stimulated genes (*B2M*, *IFIH1*, and *PARP9*), following IFN α exposure for 48 hours (Supplementary Fig. S6A–S6C). Thus, MYC overexpression selectively inhibits IFN γ signaling.

MYC-induced JAK2 silencing is dependent upon MYC/MAX heterodimerization

The MYC oncoprotein hallmark role as a transcriptional activator is well established; however, MYC is also a potent transcriptional repressor. MYC can repress a wide array of genes, most notably cell adhesion and cell-cycle inhibitory genes (47). To assess whether MYC was a direct transcriptional repressor of JAK2, we first asked whether there were MYC binding motifs in the JAK2 promoter. Indeed, query of MYC binding sites in the JAK2 promoter region using the Eukaryotic Promoter Database identified three MYC binding motifs in the JAK2 promoter (Fig. 5A). The sequence of the two proximal binding motifs is CACGCG, the most common MYC E-box variant, whereas the distal binding motif sequence is CACCTG, a less potent MYC E-box variant (48). Transfection of MYC and Mock-overexpressing cell lines with a luciferase reporter vector under the control of JAK2 promoter (JAK2 prom-Luc) demonstrated more than a 2-fold reduction in luciferase activity in MYC-overexpressing cells (paired *t* test, $P = 0.0004$; Fig. 5B). To investigate whether MYC directly inhibited JAK2 transcription, we transfected MYC-overexpressing cells with JAK2 prom-Luc vectors harboring point mutations in the three MYC binding sites (Fig. 5A). Although insertion of a point mutation in the second MYC binding site resulted in more than a 1.5-fold increase in JAK2 prom-Luc luciferase activity (paired *t* test, $P = 0.003$), point mutations in the two other MYC binding sites, alone or combined with a point mutation in the second MYC binding site, did not significantly affect luciferase activity (Fig. 5C). Replacing three nucleotides in each putative binding site yielded similar results (Supplementary Fig. S7A and S7B). Although we demonstrated that MYC directly downregulated JAK2 transcription through a specific MYC E-box variant in the JAK2 promoter, its luciferase activity level was not restored to the level observed in Mock-overexpressing cell lines, suggesting both direct and indirect JAK2 inhibition mechanisms due to MYC overexpression.

To assert that the MYC-mediated JAK2 transcriptional repression was relevant in experimental models other than MYC overexpression, we measured the effect of MYC silencing on JAK2 expression and IFN γ responsiveness. Heterodimerization of MYC with MAX (MYC-associated factor X) is essential for MYC association with E-box DNA sequences (49). Thus, we examined the effect of MYC and MAX silencing on JAK2 expression and IFN γ responsiveness. Melanoma cell lines transfected with MYC or MAX siRNA demonstrated reduced mRNA and protein expression of MYC and MAX compared with cells transfected with control siRNA (Supplementary Fig. S7C and S7D). This reduction in MYC and MAX expression was accompanied by a 2-fold upregulation in JAK2 mRNA expression (paired *t* test, $P < 0.0001$ and $P = 0.002$ for MYC and MAX, respectively; Fig. 5D). Compared with control siRNA transfected cells, MYC or MAX siRNA transfected cells demonstrated increased IFN γ responsiveness, as evident by increased mRNA expression of the IFN γ response genes *JAK2* and *IFIH1* following IFN γ exposure for 48 hours (paired *t* test,

$P < 0.01$ for all genes; Fig. 5D). Taken together, MYC or MAX silencing results in increased JAK2 expression and IFN γ responsiveness.

Finally, the success of immunotherapy is dependent upon recognition of the tumor cells by the immune system and successful antitumor T-cell effector functions. To assess the effect of MYC expression on T-cell effector functions, we measured IFN γ secretion following coculture of melanoma cells with autologous TILs in a 2.5:1 effector to target cell ratio for 18 hours. Coculture of TILs with MYC-overexpressing cells resulted in a 6-fold reduction in IFN γ secretion compared with coculture with Mock-overexpressing cells (paired *t* test, $P < 0.0001$; Fig. 5E). This inhibition of IFN γ secretion could be partially rescued by MAX silencing, as evident by a 3-fold increase in IFN γ secretion in cocultures of TILs with MYC-overexpressing melanoma cells transfected with MAX siRNA compared with cells transfected with control siRNA (paired *t* test, $P = 0.002$; Fig. 5E). We also measured IFN γ secretion from TILs cocultured with melanoma cells pretreated with the JAK2 inhibitor ruxolitinib. TILs cocultured with ruxolitinib-treated melanoma cells exhibited reduced IFN γ secretion (Supplementary Fig. S7E), similar to the reduction observed in TILs cultured with MYC-overexpressing cells. To assess the effect of MYC overexpression on tumor recognition by cytotoxic TILs, we measured the mean fluorescence intensity and percent positivity of CD8⁺ TILs for CD137 (4-1BB) and CD107a, both markers for tumor-reactive T cells (50, 51), following coculture of autologous TILs with MYC and Mock-overexpressing melanomas for 18 and 6 hours, respectively. Both TIL 53 and TIL 90 exhibited reduced expression of CD137 and CD107a in CD8⁺ TILs, whereas TIL 90 also exhibited a reduction in the percent of marker positive CD8⁺ TILs (Fig. 5F; Supplementary Fig. S8). Thus, MYC activation in melanoma cells hinders both tumor recognition and the effector functions of TILs.

In conclusion, we suggest that MYC upregulation induces a vicious cycle of melanoma-intrinsic IFN γ resistance through MYC/MAX heterodimerization-dependent repression of JAK2 transcription, combined with reduced TIL effector function and IFN γ secretion, thus cumulating in inhibition of the antitumor immune response and immunotherapy failure.

Discussion

Because the introduction of immunotherapy as a pillar of advanced melanoma treatment, numerous articles have tried to unravel the mechanisms that govern the response and resistance to immunotherapy. Although there is a growing consensus that high tumor mutational load, TILs, IFN γ signaling, and upregulation of the antigen processing and presentation pathway are all critical for immunotherapy response (52), the mechanisms which govern the resistance to immunotherapy are still largely unknown. Although several oncogenic pathways such as WNT/ β -catenin, cyclin-dependent kinase 4/6, and the mitogen-activated kinase pathways were implicated as deterrents to immunotherapy (15), we are still unable to predict which patients will benefit from immunotherapy. To further investigate the pathways associated with immunotherapy response and resistance, we performed both proteome (17) and transcriptome profiling of preimmunotherapy tumor biopsies from patients with advanced melanoma treated with either TIL ACT or PD-1 blockade. We identified three distinct gene clusters which differentiated responders from nonresponders to immunotherapy—Melanoma response and Leukocyte marker gene clusters, which were upregulated in responders and were enriched for immune-related pathways such as immune effector process and IFN response genes, and the Melanoma resistance gene

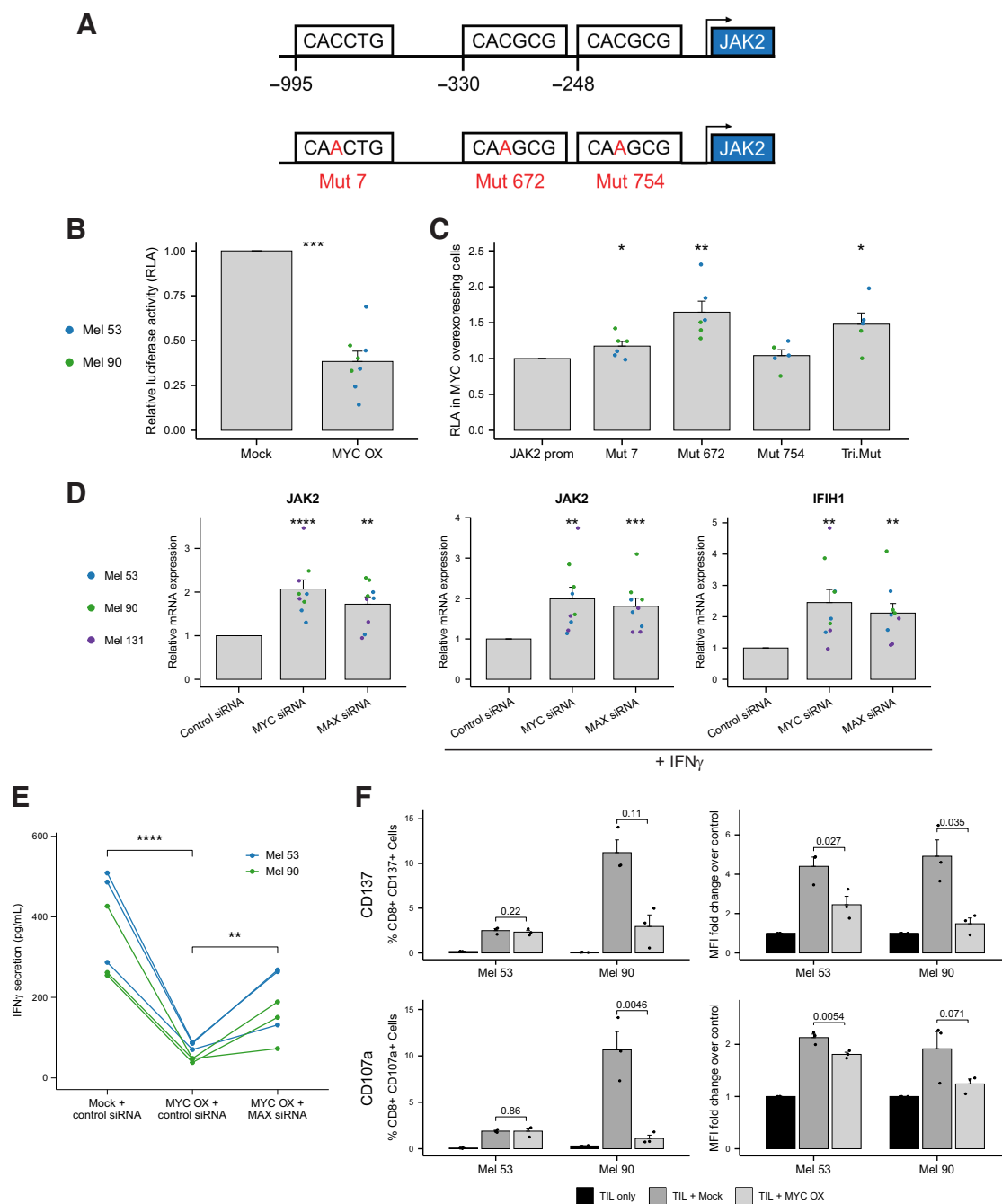


Figure 5.

MYC induces JAK2 transcription downregulation and IFN γ resistance through MYC-MAX heterodimerization. **A**, Top: MYC binding motifs within the JAK2 promoter. Bottom: Point mutations (C to A) inserted into the three MYC binding motifs within the JAK2 promoter. **B**, Luciferase activity of MYC and Mock-overexpressing cells transfected with a luciferase reporter vector under the control of JAK2 promoter (JAK2 prom-Luc). Each line represents a single experiment. All firefly luciferase activity measurements in **B** and **C** were normalized to *Renilla* luciferase activity as an internal control. **C**, Luciferase activity of MYC-overexpressing cells transfected with JAK2 prom-Luc vectors harboring point mutations (C to A) in the three MYC binding sites [mut 7, mut 672, mut 754, and triple mutant (Tri.Mut)] relative to cells transfected with a wild-type JAK2 prom-Luc vector (JAK2 prom). **D**, Relative mRNA expression via qRT-PCR of the IFN γ response genes JAK2 and IFIH1 in melanoma cell lines 72 hours after transfection with MYC, MAX, or control siRNA. Middle and right: 24 hours following siRNA transfection, cells were exposed to 10 ng/mL of IFN γ for 48 hours. **E**, IFN γ secretion in supernatant of Mel 53 and Mel 90 MYC and Mock-overexpressing cells coincubated with autologous TILs in a 2.5:1 effector to target cell ratio for 18 hours assessed via ELISAs. 24 hours prior to coinocubation with TILs, melanoma cells were transfected with control or MAX siRNA. Each line represents a single experiment. **F**, Left: Percent of CD8⁺ TILs positive for CD137 (4-1BB) or CD107a in Mel 53 and Mel 90 MYC and Mock-overexpressing cells coincubated with autologous TILs in a 2.5:1 effector to target cell ratio for 18 and 6 hours, respectively, assessed via flow cytometry. Right: The mean fluorescence intensity (MFI) fold change over control of CD137 and CD107a in CD8⁺ TILs. *P* values in **B-F** were computed using a paired *t* test. Bar plot data are represented as mean + SE, where each dot represents a single experiment. *, *P* < 0.05; **, *P* < 0.01; ***, *P* < 0.001; ****, *P* < 0.0001.

cluster, which was downregulated in responders and enriched for oncogenic pathways such as cell cycle and dedifferentiation. These results are in agreement with several other articles that identify IFN γ signaling, immune infiltration, and oncogenic pathways as major determinants for immunotherapy outcome (10, 12–16). The Melanoma response and IFN resistance gene clusters were strongly inversely correlated in several melanoma bulk RNA-seq datasets, as well as within a scRNA-seq dataset of melanoma cells (16, 25), and exhibited comparable or better performance as predictors of overall survival in immunotherapy-treated patients than tumor immune cell infiltration assessed by gene expression signatures. Using IPA upstream regulator analysis, we identified IFN γ and MYC as the major transcription regulators associated with the Melanoma response and resistance gene clusters, respectively. Furthermore, MYC nuclear staining was upregulated in melanoma pretreatment tumor biopsies of nonresponders to PD-1 blockade. Thus, we identified two melanoma-intrinsic and mutually exclusive gene programs that were controlled by IFN γ and MYC and the relationship to immunotherapy outcome.

Although IFN γ is a known key mediator of antitumor immunity and immunotherapy response through activation of JAK-STAT signaling (11, 13), the role of MYC in immunotherapy resistance is largely unknown. MYC, one of the most common deregulated oncogenes in a wide variety of cancers (53), is involved in both tumor initiation and maintenance through several mechanisms, including increased cellular proliferation and growth, enhanced transcription and protein synthesis, blocking of differentiation, altered cellular metabolism, and activation of angiogenesis (54). Another important MYC function in tumorigenesis was highlighted, as MYC was found to modulate immune regulatory molecules, thereby contributing to suppression of antitumor immune responses (55). A recent article detected enrichment for MYC targets in a scRNA-seq profiles of immune checkpoint-resistant melanoma tumors (16), and other publications have demonstrated that inhibiting MYC signaling through a direct inhibitor or through epigenetic therapies can reverse immune evasion and sensitize tumors to immunotherapy (56, 57). A recent article has also identified several transcriptional programs, including CTNNB1, KLF4, HIF1A, sonic hedgehog, and MYC as particularly important, as these programs associated with immune exclusion in a pan-cancer analysis (53). Interestingly, the authors suggest substantial cross-talk between those pathways and an additive impact on immune exclusion across cancers, with MYC signaling identified as perhaps the most important node associated with immune exclusion. Taken together with a recent review, which identifies MYC as a global regulator of immune responses (58), it is possible that oncogenic pathway converge through MYC activation to elicit immune exclusion and immunotherapy resistance.

Although several recent articles identify MYC as a facilitator of immune exclusion, how MYC induces immunotherapy resistance is largely unknown. Here, we present a novel mechanism of MYC-induced immunotherapy resistance through an inhibitory effect on JAK2, an important protein in the IFN γ signaling cascade. MYC-overexpressing cells from Immune low, patient-derived melanoma cell lines exhibited a significant reduction in IFN γ responsiveness, which associated with downregulation of JAK2 expression. We additionally observed reduced luciferase activity in MYC-overexpressing cells transfected with a luciferase reporter vector under the control of JAK2 promoter. This reduction in luciferase activity was partially reversed upon insertion of a point mutation in the second MYC E-box binding site identified in the JAK2 promoter. Further solidifying the relationship between MYC activation, JAK2 downregulation, and immuno-

therapy resistance, we detected that inhibition of MYC or its cofactor MAX through siRNA targeting resulted in increased JAK2 expression and IFN γ responsiveness of transfected cells. Finally, we observed reduced tumor recognition and T-cell effector functions in autologous TILs cocultured with MYC-overexpressing melanomas, which were partially rescued by MAX silencing. These findings shed light on a new immunotherapy and IFN γ resistance mechanism and suggest that immunotherapy-resistant patients might benefit from a combination of immunotherapy and MYC inhibiting drugs.

Several articles that profiled the transcriptomes of responders and nonresponders to immunotherapy report an association between preexisting immune activation gene signatures and clinical benefit (10, 12, 22, 23). In agreement, we describe immune infiltration as a favorable feature associated with immunotherapy response. However, we suggest that the two melanoma-intrinsic mutually exclusive cell programs, which are regulated by IFN γ and MYC, are also of great importance to immunotherapy outcome. Our dataset is unique as we provide the first immunotherapy cohort with both transcriptome and proteome (17) profiling. Whereas the major advantage of proteomic profiling is that it quantifies the main functional molecules of the cells, we utilized the deep coverage of RNA-seq to complement the previous proteomic findings and to better assess the importance of immune-related and lowly expressed genes, such as cytokines, signal transduction molecules, and immune cell activation, to immunotherapy outcome. In concordance with a previously published article (37), we report that protein levels of proteins involved in induced processes such as epithelial–mesenchymal transition, hypoxia, and IFN signaling are mostly regulated by mRNA abundance, whereas protein levels for cell homeostasis processes are mostly posttranscriptional, as reflected by enrichment for these processes in cells with low correlation between protein and mRNA levels.

In conclusion, we report the identification of two mutually exclusive melanoma-intrinsic gene programs that represent IFN γ response and resistance and the association with immunotherapy outcome. We identified MYC as the major transcription regulator associated with IFN γ resistance through JAK2 transcription inhibition. Thus, further research on the effect of MYC inhibition in immunotherapy-resistant patients is warranted to improve the clinical outcomes of these patients.

Authors' Disclosures

E. Markovits reports personal fees from Nucleai outside the submitted work. T. Geiger reports grants from Israel Science Foundation during the conduct of the study. G. Markel reports personal fees from Roche, MSD, Nucleai, Beyond Air, Biond Biologics, Biomica, Starget, and 4cBiomed; grants and personal fees from Novartis, BMS, Medison, and Sanofi outside the submitted work; and is founder and chief scientific officer of 4c BioMed; SAB member of Biomica, Biond Biologics, Nucleai; and senior medical advisor of Starget. No disclosures were reported by the other authors.

Authors' Contributions

E. Markovits: Conceptualization, data curation, software, formal analysis, validation, investigation, visualization, methodology, writing-original draft, project administration, writing-review and editing. **O. Harush:** Formal analysis, investigation, methodology. **E.N. Baruch:** Data curation. **E.D. Shulman:** Resources, formal analysis. **A. Debby:** Resources, data curation, formal analysis, investigation. **O. Itzhaki:** Data curation. **L. Anafi:** Data curation. **A. Danilevsky:** Resources. **N. Shomron:** Resources, funding acquisition. **G. Ben-Betzalel:** Resources, data curation. **N. Asher:** Resources, data curation. **R. Shapira-Frommer:** Resources, data curation. **J. Schachter:** Resources, data curation. **I. Barshack:** Resources, data curation. **T. Geiger:** Conceptualization, resources, supervision. **R. Elkou:** Resources, data curation. **M.J. Besser:** Conceptualization, resources, data curation, funding acquisition. **G. Markel:** Conceptualization, resources, data curation, supervision, funding acquisition, project administration.

Acknowledgments

This work was supported by the Melanoma Research Alliance Saban Family Team Science Award and Kamin grant of the Israel Innovation Authority to T. Geiger, N. Shomron, and G. Markel and the Samueli Foundation Grant for Integrative Immuno-Oncology and ISF 3956/19 (IPMP) to G. Markel. Special thanks for the Lemelbaum Family, Aronson Foundation, and Allen Berg Fund for Excellence in Immuno-Oncology for their generous support. The results shown here are in part based upon data generated by TCGA Research Network: <https://www.cancer.gov/tcga>. This study was part of E. Markovits and O. Harush's PhD thesis in the Department of Clinical Immunology and Microbiology at the Sackler Faculty of Medicine, Tel Aviv University.

The publication costs of this article were defrayed in part by the payment of publication fees. Therefore, and solely to indicate this fact, this article is hereby marked "advertisement" in accordance with 18 USC section 1734.

Note

Supplementary data for this article are available at Cancer Immunology Research Online (<http://cancerimmunolres.aacrjournals.org/>).

Received March 18, 2022; revised November 27, 2022; accepted April 17, 2023; published first April 18, 2023.

References

- Sharma P, Allison JP. The future of immune checkpoint therapy. *Science* 2015; 348:56–61.
- Sharma P, Allison JP. Immune checkpoint targeting in cancer therapy: toward combination strategies with curative potential. *Cell* 2015;161:205–14.
- Homet Moreno B, Ribas A. Anti-programmed cell death protein-1/ligand-1 therapy in different cancers. *Br J Cancer* 2015;112:1421–7.
- Schumacher TN, Schreiber RD. Neoantigens in cancer immunotherapy. *Science* 2015;348:69–74.
- Larkin J, Chiarion-Sileni V, Gonzalez R, Grob JJ, Rutkowski P, Lao CD, et al. Five-year survival with combined nivolumab and ipilimumab in advanced melanoma. *N Engl J Med* 2019;381:1535–46.
- Rosenberg SA, Restifo NP, Yang JC, Morgan RA, Dudley ME. Adoptive cell transfer: a clinical path to effective cancer immunotherapy. *Nat Rev Cancer* 2008; 8:299–308.
- Besser MJ, Shapira-Frommer R, Treves AJ, Zippel D, Itzhaki O, Hershkovitz L, et al. Clinical responses in a phase II study using adoptive transfer of short-term cultured tumor infiltration lymphocytes in metastatic melanoma patients. *Clin Cancer Res* 2010;16:2646–55.
- Besser MJ, Shapira-Frommer R, Itzhaki O, Treves AJ, Zippel DB, Levy D, et al. Adoptive transfer of tumor-infiltrating lymphocytes in patients with metastatic melanoma: intent-to-treat analysis and efficacy after failure to prior immunotherapies. *Clin Cancer Res* 2013;19:4792–800.
- Johnson DB, Frampton GM, Rioth MJ, Yusko E, Xu Y, Guo X, et al. Targeted next generation sequencing identifies markers of response to PD-1 blockade. *Cancer Immunol Res* 2016;4:959–67.
- Gide TN, Quek C, Menzies AM, Tasker AT, Shang P, Holst J, et al. Distinct immune cell populations define response to anti-PD-1 monotherapy and anti-PD-1/Anti-CTLA-4 combined therapy. *Cancer Cell* 2019;35:238–55.
- Ayers M, Lunceford J, Nebozhyn M, Murphy E, Loboda A, Kaufman DR, et al. IFN- γ -related mRNA profile predicts clinical response to PD-1 blockade. *J Clin Invest* 2017;127:2930–40.
- Liu D, Schilling B, Liu D, Sucker A, Livingstone E, Jerby-Amon L, et al. Integrative molecular and clinical modeling of clinical outcomes to PD1 blockade in patients with metastatic melanoma. *Nat Med* 2019;25:1916–27.
- Zaretsky JM, Garcia-Diaz A, Shin DS, Escuin-Ordinas H, Hugo W, Hu-Lieskovan S, et al. Mutations associated with acquired resistance to PD-1 blockade in melanoma. *N Engl J Med* 2016;375:819–29.
- Spranger S, Bao R, Gajewski TF. Melanoma-intrinsic β -catenin signalling prevents anti-tumour immunity. *Nature* 2015;523:231–5.
- Kalbasi A, Ribas A. Tumour-intrinsic resistance to immune checkpoint blockade. *Nat Rev Immunol* 2020;20:25–39.
- Jerby-Aron L, Shah P, Cuoco MS, Rodman C, Su MJ, Melms JC, et al. A cancer cell program promotes T cell exclusion and resistance to checkpoint blockade. *Cell* 2018;175:984–97.
- Harel M, Ortenberg R, Varanasi SK, Mangalharra KC, Mardamshina M, Markovits E, et al. Proteomics of melanoma response to immunotherapy reveals mitochondrial dependence. *Cell* 2019;179:236–50.
- Besser MJ, Shapira-Frommer R, Treves AJ, Zippel D, Itzhaki O, Schallmach E, et al. Minimally cultured or selected autologous tumor-infiltrating lymphocytes after a lympho-depleting chemotherapy regimen in metastatic melanoma patients. *J Immunother* 2009;32:415–23.
- Dobin A, Davis CA, Schlesinger F, Drenkow J, Zaleski C, Jha S, et al. STAR: ultrafast universal RNA-seq aligner. *Bioinformatics* 2013;29:15–21.
- Liao Y, Smyth GK, Shi W. FeatureCounts: an efficient general purpose program for assigning sequence reads to genomic features. *Bioinformatics* 2014;30:923–30.
- Law CW, Chen Y, Shi W, Smyth GK. Voom: precision weights unlock linear model analysis tools for RNA-seq read counts. *Genome Biol* 2014;15:R29.
- Riaz N, Havel JJ, Makarov V, Desrichard A, Urba WJ, Sims JS, et al. Tumor and microenvironment evolution during immunotherapy with nivolumab. *Cell* 2017;171:934–49.
- Lauss M, Donia M, Harbst K, Andersen R, Mitra S, Rosengren F, et al. Mutational and putative neoantigen load predict clinical benefit of adoptive T cell therapy in melanoma. *Nat Commun* 2017;8:1738.
- Hugo W, Zaretsky JM, Sun L, Song C, Moreno BH, Hu-Lieskovan S, et al. Genomic and transcriptomic features of response to anti-PD-1 therapy in metastatic melanoma. *Cell* 2017;168:542.
- Tirosh I, Izar B, Prakadan SM, Wadsworth MH, Treacy D, Trombetta JJ, et al. Dissecting the multicellular ecosystem of metastatic melanoma by single-cell RNA-seq. *Science* 2016;352:189–96.
- Yoshihara K, Shahmoradgoli M, Martinez E, Vegesna R, Kim H, Torres-Garcia W, et al. Inferring tumour purity and stromal and immune cell admixture from expression data. *Nat Commun* 2013;4:2612.
- Subramanian A, Tamayo P, Mootha VK, Mukherjee S, Ebert BL, Gillette MA, et al. Gene set enrichment analysis: a knowledge-based approach for interpreting genome-wide expression profiles. *Proc Natl Acad Sci U S A* 2005;102:15545–50.
- Liberzon A, Birger C, Thorvaldsdóttir H, Ghandi M, Mesirov JP, Tamayo P. The molecular signatures database hallmark gene set collection. *Cell Syst* 2015;1: 417–25.
- Aran D, Hu Z, Butte AJ. xCell: digitally portraying the tissue cellular heterogeneity landscape. *Genome Biol* 2017;18:220.
- Hänzelmann S, Castelo R, Guinney J. GSEA: gene set variation analysis for microarray and RNA-seq data. *BMC Bioinformatics* 2013;14:7.
- Cerami E, Gao J, Dogrusoz U, Gross BE, Sumer SO, Aksoy BA, et al. The cBio cancer genomics portal: an open platform for exploring multidimensional cancer genomics data. *Cancer Discov* 2012;2:401–4.
- Itzhaki O, Hovav E, Ziporen Y, Levy D, Kubi A, Zikich D, et al. Establishment and large-scale expansion of minimally cultured "Young" tumor infiltrating lymphocytes for adoptive transfer therapy. *J Immunother* 2011;0:212–20.
- Greenberg E, Hershkovitz L, Itzhaki O, Hajdu S, Nemlich Y, Ortenberg R, et al. Regulation of cancer aggressive features in melanoma cells by microRNAs. *PLoS One* 2011;6:e18936.
- Dreos R, Ambrosini G, Périer RC, Bucher P. The Eukaryotic Promoter Database: expansion of EPDNew and new promoter analysis tools. *Nucleic Acids Res* 2015; 43:D92–6.
- Wang X, Slebos RJC, Wang D, Halvey PJ, Tabb DL, Liebler DC, et al. Protein identification using customized protein sequence databases derived from RNA-seq data. *J Proteome Res* 2012;11:1009–17.
- Wang X, Liu Q, Zhang B. Leveraging the complementary nature of RNA-seq and shotgun proteomics data. *Proteomics* 2014;14:2676–87.
- Jovanovic M, Rooney MS, Mertins P, Przybylski D, Chevrier N, Satija R, et al. Dynamic profiling of the protein life cycle in response to pathogens. *Science* 2015;347:1259038.
- Hemesath TJ, Steingrimsson E, McGill G, Hansen MJ, Vaught J, Hodgkinson CA, et al. microphthalmia, a critical factor in melanocyte development, defines a discrete transcription factor family. *Genes Dev* 1994;8:2770–80.

39. Chen G, Wang H, Miller CT, Thomas DG, Gharib TG, Misek DE, et al. Reduced selenium-binding protein 1 expression is associated with poor outcome in lung adenocarcinomas. *J Pathol* 2004;202:321–9.
40. Cairo S, Armengol C, De Reyniès A, Wei Y, Thomas E, Renard C-A, et al. Hepatic stem-like phenotype and interplay of Wnt/beta-catenin and Myc signaling in aggressive childhood liver cancer. *Cancer Cell* 2008;14:471–84.
41. Zingg D, Arenas-Ramirez N, Sahin D, Rosalia RA, Antunes AT, Haeusel J, et al. The histone methyltransferase Ezh2 controls mechanisms of adaptive resistance to tumor immunotherapy. *Cell Rep* 2017;20:854–67.
42. Neri F, Zippo A, Krepelova A, Cherubini A, Rocchigiani M, Oliviero S. Myc regulates the transcription of the PRC2 gene to control the expression of developmental genes in embryonic stem cells. *Mol Cell Biol* 2012;32:840–51.
43. Osanto S, Jansen R, Vloemans M. Downmodulation of c-myc expression by interferon γ and tumour necrosis factor α precedes growth arrest in human melanoma cells. *Eur J Cancer* 1992;28:1622–7.
44. Bahram F, Hydbring P, Tronnorsjö S, Zakaria SM, Frings O, Fahlén S, et al. Interferon- γ -induced p27KIP1 binds to and targets MYC for proteasome-mediated degradation. *Oncotarget* 2016;7:2837–54.
45. Garcia-Diaz A, Shin DS, Moreno BH, Saco J, Escuin-Ordinas H, Rodriguez GA, et al. Interferon receptor signaling pathways regulating PD-L1 and PD-L2 expression. *Cell Rep* 2017;19:1189–201.
46. Lin R-J, Liao C-L, Lin E, Lin Y-L. Blocking of the alpha interferon-induced jak-stat signaling pathway by Japanese encephalitis virus infection. *J Virol* 2004;78:9285–94.
47. Herkert B, Eilers M. Transcriptional repression: The dark side of Myc. *Genes Cancer* 2010;1:580–6.
48. Allevalo M, Bolotin E, Grossman M, Mane-Padros D, Sladek FM, Martinez E. Sequence-specific DNA binding by MYC/MAX to low-affinity non-E-box motifs. *PLoS One* 2017;12:e0180147.
49. Amati B, Brooks MW, Levy N, Littlewood TD, Evan GI, Land H. Oncogenic activity of the c-Myc protein requires dimerization with Max. *Cell* 1993;72:233–45.
50. Betts MR, Brenchley JM, Price DA, De Rosa SC, Douek DC, Roederer M, et al. Sensitive and viable identification of antigen-specific CD8+ T cells by a flow cytometric assay for degranulation. *J Immunol Methods* 2003;281:65–78.
51. Seliktar-Ofir S, Merhavi-Shoham E, Itzhaki O, Yunger S, Markel G, Schachter J, et al. Selection of shared and neoantigen-reactive T cells for adoptive cell therapy based on CD137 separation. *Front Immunol* 2017;8:1211.
52. Havel JJ, Chowell D, Chan TA. The evolving landscape of biomarkers for checkpoint inhibitor immunotherapy. *Nat Rev Cancer* 2019;19:133–50.
53. Bao R, Stapor D, Luke JJ. Molecular correlates and therapeutic targets in T cell-inflamed versus non-T cell-inflamed tumors across cancer types. *Genome Med* 2020;12:90.
54. Gabay M, Li Y, Felsner DW. MYC activation is a hallmark of cancer initiation and maintenance. *Cold Spring Harb Perspect Med* 2014;4:a014241.
55. Casey SC, Tong L, Li Y, Do R, Walz S, Fitzgerald KN, et al. MYC regulates the antitumor immune response through CD47 and PD-L1. *Science* 2016;352:227–31.
56. Han H, Jain AD, Truica MI, Izquierdo-Ferrer J, Anker JF, Lysy B, et al. Small-molecule MYC inhibitors suppress tumor growth and enhance immunotherapy. *Cancer Cell* 2019;36:483–97.
57. Topper MJ, Vaz M, Chiappinelli KB, DeStefano Shields CE, Niknafs N, Yen RWC, et al. Epigenetic therapy ties MYC depletion to reversing immune evasion and treating lung cancer. *Cell* 2017;171:1284–300.
58. Casey SC, Baylot V, Felsner DW. The MYC oncogene is a global regulator of the immune response. *Blood* 2018;131:2007–15.